XLIII CILAMCE
21–25, November, 2022
FOZ DO IGUAÇU – PR – BRAZIL

Application of a neural architecture to estimate the wear of down and up throats in RH degassers

Lucas M. Ayres[1], Pablo F. Salarolli[1], Leonardo G. Batista[1], Eric N. de Almeida[1], Gustavo M. de Almeida[1], Marco A. S. L. Cuadros[1]

[1]*Master's program in control and automation engineering, Federal Institute of Espírito Santo*
Av. dos Sabiás, 330 - Morada de Laranjeiras, 29166-630, Serra-ES, Brazil
lucmantuan@gmail.com, pablosalarolli@gmail.com, leonardo-baptista@live.com, ericnovaesdealmeida@gmail.com, gmaia@ifes.edu.br, marcoantonio@ifes.edu.br

Abstract. During the metallurgical process of steelmaking, conformity is achieved in the processes of primary and secondary refining. One of the types of secondary refining takes place in the RH degasser, where the molten steel from primary refining is fed into a ladle below RH. RH and the ladle are connected by two tubes called "up leg" and "down leg". The steel is encouraged to circulate in the up leg, while the molten bath flows back into the ladle through the down leg. The edges of the refractory bricks of both legs, also called "throats," are subject to wear. This observation is made by an operator who goes to the top of the degassing ladle and uses a cell phone to take a picture of the condition of the throats on the lower vessel of RH. The image is evaluated to check for throat wear and to ensure the integrity of the process to avoid perforations and unavailability of RH. To provide a more meaningful measurement, YOLACT, a neural architecture designed for real-time image segmentation, is used to extract the coordinates describing the segmentation of the throats in the images, which are later processed to estimate the actual wear.

Keywords: RH refractory erosion, RH refractory wear, computational vision, instance segmentation, YOLACT.

1 Introduction

The process of obtaining molten steel can be summarized in two stages: pig iron production and molten production. is obtained. First, it is obtaining the pig iron a metallic material that is produced in the blast furnace and consists of iron and a high proportion of carbon and impurities. The pretreatment of the pig iron consists in ensuring that the composition of the material is appropriate and that silicon (Si), phosphorus (P) and sulfur (S) are removed. The pig iron is then subjected to the steel refining process (primary refining), which is carried out by the controlled oxidation of impurities in the pig iron and in the scrap, which is also fed to the process, as Torres [1] states. Although sulfur is reduced during pig iron pretreatment, additional desulfurization (de-S) is required for some grades of steel (S < 10ppm) used, for example, in the marine and aerospace markets. In order to achieve low sulfur content, lower carbon content and reduction of gasses (hydrogen, nitrogen and oxygen), this treatment is carried out in secondary refining, usually using the RH vacuum degasser, which is widely used in steel treatment according to Silveira [2] and Silva et al [3]. In this process sequence, the molten steel from the primary refining is placed in a ladle located under the degassing vessel. In the work of [2] , it is highlighted that the vessel has at its bottom two refractory tubes, called up leg and down leg, respectively, which serve to promote the circulation of the steel between the vessel and the ladle and, consequently, the decarburization and degassing of the steel. Among the possible wear phenomena of the RH vessel refractory, the erosion caused by the increase in the circulation velocity of the molten steel is the most aggressive for the life of the refractory, especially at the upper edges of the up leg and down leg, the so-called throats, as presented by Melo et al [4]. Wear is monitored by an operator who goes to the top of the vessel and records the condition of the throats with a photo camera through the tube into which the oxygen lance, used in the decarburization process, is lowered. The image is analyzed to estimate the life of the refractory, focusing on the integrity of the vessel, which can be perforated. When the wear reaches the

specified limit, the RH process is interrupted to replace new refractory bricks. This method exposes the operator to high nozzle temperatures, which jeopardizes his operational safety. In addition, wear analysis is not performed online, which means that a time interval after image acquisition is required so that the techniques currently used for estimation can be used by the responsible personnel.

In this way, this work presents a method not mentioned in other works that uses a convolutional model for the segmentation of images in real time, with the proposal to help in the monitoring of wearing, to help reduce the operator's exposure to the high temperatures, and, when embedded in a monitoring system, to be able to process and provide estimates online. This model is YOLACT, the output of which (images showing the segmented wear area) is processed to delineate the segmentation contour. The coordinates of the contour in pixels are known and are used to calculate the largest distance between pixels in this set. Then, this result is related to the actual distance measurements to obtain an estimate of the maximum wear of the throats.

2 RH Degasser

The Ruhrstahl-Heraeus degassing process (RH) is used to remove gaseous impurities such as hydrogen and nitrogen, which have a detrimental effect on steel mechanics at the end of the production line. In addition, reactions between carbon and oxygen are accelerated at low pressures, so that a high decarburization rate can be achieved. In this process, it is possible to remove part of the inclusions contained in the liquid steel and promote the homogenization of the chemical composition and temperature, as Vieira [5] points out.

Based on the work of Morais et al [6] and Maranhão [7], the process of vacuum degassing is described below, which is visually represented in Fig. 1 adapted from Marchesi [8]:

The ladle filled with molten steel is lifted and positioned under the vessel; the up and down legs are introduced into the metal bath; pressure reduction is promoted in the upper vessel by the vacuum chamber, causing the molten steel to rise about 1.40 m above the original surface level due to the pressure difference in the vessel and ladle; when the gas (typically argon) comes into contact with the metal bath, it experiences a large increase in volume due to the increase in temperature and the decrease in pressure, so that the molten steel inside the vessel experiences a difference in height that depends on the argon flow. The gas causes a decrease in the apparent density of the steel in the up leg, while in the down leg the apparent density remains unchanged; the difference in density between the legs promotes the circulation of the molten steel; the steel flow, containing gas bubbles, is moved at high speed into the vessel, dispersing the steel droplets and releasing the gases dissolved in the metal bath; in this way, the circulation of the steel and the subsequent continuous degassing take place; at the end of the process, the chemical composition, temperature and oxygen content are measured. After the measurements and considering the previously established limits, the molten steel is sent to continuous casting.

3 YOLACT

In the field of computer vision, there are notable applications related to image and video processing. Of these, three stand out: image classification, object detection, and image segmentation, which can be divided into semantic segmentation and instance segmentation in the context of convolutional neural networks. The works of González [9], Kutyonen [10] and Tabares [11] define these applications as follows, exemplified in Fig. 2 from Liu et al. [12].

- Image classification: this is one of the essential problems of modern computer vision, where the goal is to create a model that can classify one or more images into a set of predefined classes, i.e., the classification determines which objects are present in the images.
- Object detection: the next task combines classification and localization to determine which class is recognized and in which region of the image the object is located, delineated by a bounding box.
- Semantic segmentation: semantic segmentation is described as the process of classifying the pixels of an image into a particular class, dividing the image into regions with the shape and edge of the objects present; it is important to note that different instances of the same class are not separated here, as shown
- Instance segmentation: the result of this process is a group of regions covering the shapes of each object. Instance segmentation distinguishes instances of the same class.

The proposed architectures for instance segmentation applications, run into an obstacle when it comes to the

real-time performance that is sometimes required for devices that require minimal response times and decision making. In this context, the Mask-R CNN (Gkioxari, Dollar and Girshik [13]), the FCIS (Li et al [14]), the RetinaMask (Fu, Shvets and Berg [15]) and PA-Net (Liu et al [16]) are examples that have relatively good performance, but their inferences cannot be used in "real time" due to the high computational complexity involved in creating such systems; the large number of parameters makes it impossible for these networks to run on machines with lower computational power. The task therefore requires a different architecture capable of performing the computations in "real time", as Kanjee notes [17]. YOLACT, developed by Bolya [18], is an optimized version for instance segmentation and has gained a reputation for its speed and accuracy advantages, being able to achieve 29.8 mAP (mean Average Precison) on MS COCO at 33 frames per second, which is much faster than other competing frameworks due to its one-stage instance segmentation model.

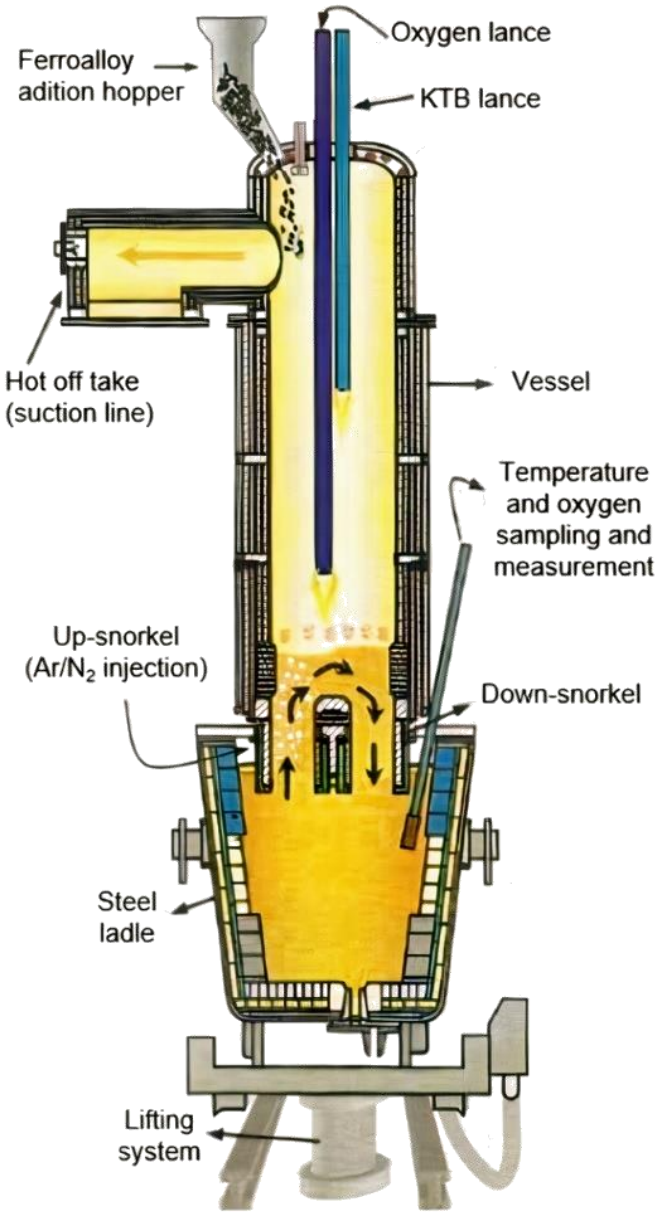

Figure 1. RH vacuum degassing process

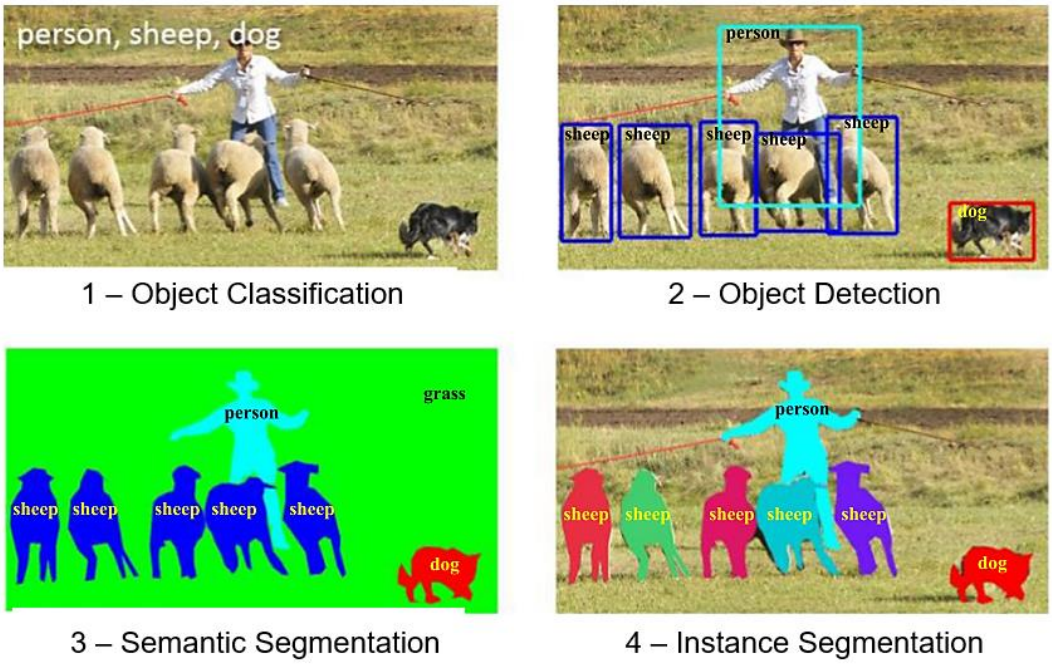

Figure 2. Computer vision tasks

In the scenario of this work, YOLACT has been chosen because of the points discussed above, highlighting its speed, superior to other structures, and suitable for the approach presented here, which is to present a model that can be embedded in a system for online estimations.

4 Methodology

4.1 Dataset

The dataset used to train the YOLACT model consists of one hundred images, 90% used for training and 10% for validation. This dataset was formed after selecting four frames from a video provided by a steel company, taken perpendicular to the throats. The 11-second video, with a frame rate of 30 frames per second, was taken with a cell phone camera whose model is unknown. Only these four images captured the two throats of the lower vessel of the RH degasser, and through them artificially altered images of the original ones were created. For this purpose, we used the Python library Augmentor, presented by Bloice [19], which provides refined control over the automation of image augmentation and implements the main real-world techniques for generating artificial images. The user selects the desired operations to modify the original set and generate new images, specifying a probability to decide whether to apply an operation to an image as it passes through the augmentation pipeline. The settings of the applied operations are accessible in the code implemented in Notebook Colab, which can be viewed in the Mantuan repository [20].

Figure 3 shows four examples from the set of one hundred generated images, all with the same resolution of 960 x 1280 pixels and different properties of brightness, distortion, and orientation randomly determined by the user at predefined intervals.

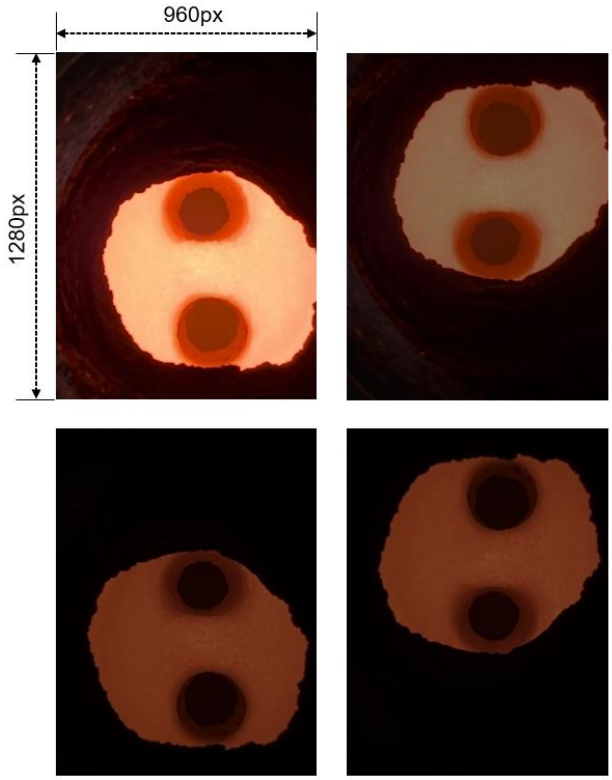

Figure 3. Examples of the generated artificial dataset

4.2 Extracting Segmentation Results

Figure 4 shows the steps applied to extract the distance (in pixels) of the validation images from the dataset. The first stage includes the evaluation of the model trained with 100 epochs and a batch size of 1. The mAP metrics of the trained model are in Tab. 1. In this stage, the ten images go through this process with a confidence threshold of 0.3 and the result is the delineation of the pixels (masks) of the instances identified by the model. Since this is an instance segmentation, the instances of the throat class are distinguished. In the example of Fig. 4, the mask of the first instance is blue and that of the second is red, and the labels have an identifier index and a score relating the predicted mask to the ground truth. If the score is equal to 1, both masks overlap. In the second stage, the masks are binarized, i.e., the pixels that mark the region of interest in the image become white. The other pixels are black by default. In the third stage, the binarized images are subjected to the edge detection method, which provides the coordinates (x,y) in pixels for each point of the mask contour, shown in a magenta tone in Fig. 4. All coordinates are stored so that later the largest Euclidean distance between the elements of the set can be calculated. After the calculation, the line between the farthest contour pixels is drawn. In the fourth stage, the lines are plotted on the masks resulting from the first stage, with dimensions 333.53 pixels and 302.72 pixels for the first (throat 1) and second (throat 2) instances, respectively, in the example in Fig. 4.

Table 1. Mask mAP results

	Backbone	mAP	mAP_{50}	mAP_{75}	mAP_{90}	mAP_{95}
Mask	ResNet101	92.21	100	100	100	22.09

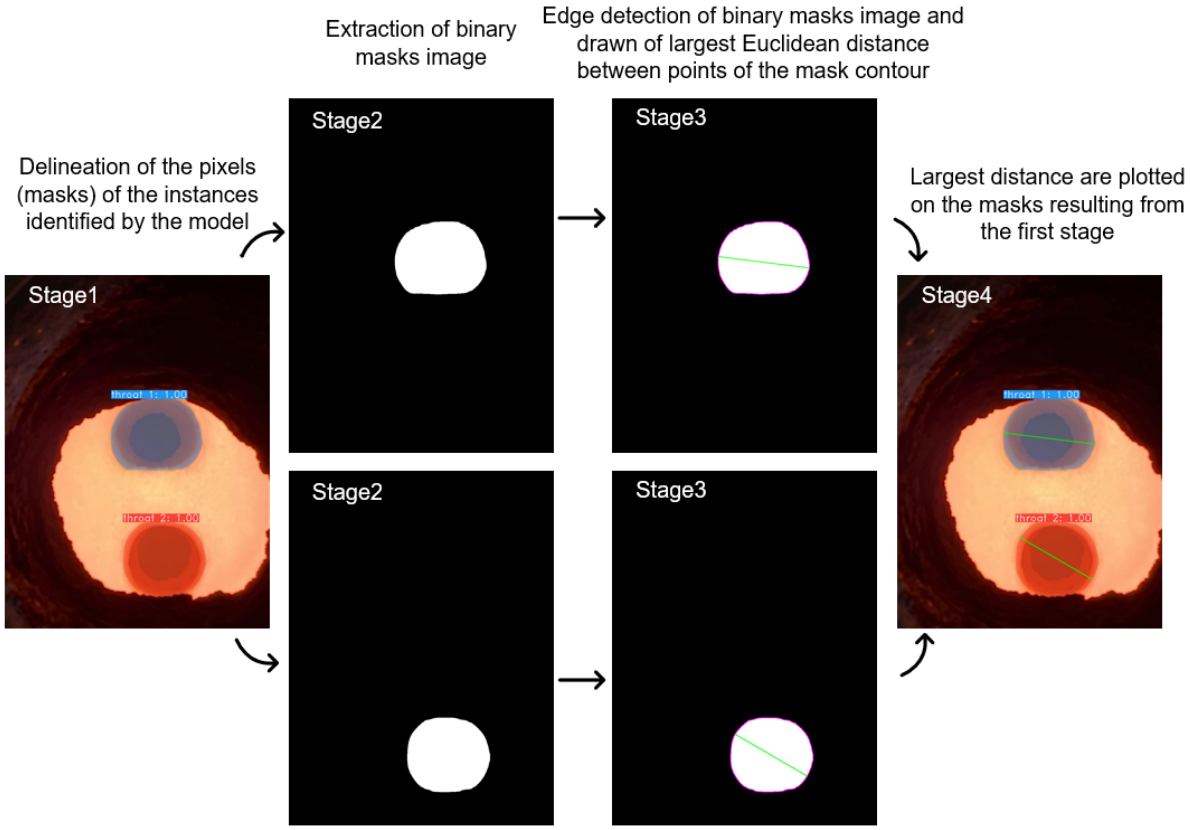

Figure 4. Stages to extract maximum wear of the throats

4.3 Estimation of real wear

By determining the maximum wear in pixel units, it is possible to relate it to the real metric system, using SI units. The refractory bricks of the lower vessel of the RH degasser, when not wore, correspond to the original diameter of the up-throat and down-throat, i.e., 0.572 m, according to the company. In Fig. 4, it was estimated that this value corresponds to 188 pixels. Therefore, it is possible to mathematically relate these units and deduce that the largest Euclidean distances for the first and second instances are 1.014 m and 0.921 m, respectively. With these data, the relative wear is extracted with respect to the original refractory by subtracting 0.572 m from the calculated distances, and with these parameters, operators can predict the number of heats before replacing the refractory.

5 Conclusions

The description of the method shown in this paper is a way to present the company with a computer vision tool that eliminates the need for all the manual calculations and spreadsheets currently used to evaluate throat images and is capable of assisting in monitoring refractory wear and reducing employee exposure to the operating environment of the RH degasser. The trained model, based on a widely accepted structure in the state-of-art, can be embedded in a refractory monitoring system to display indirectly taken measurements online. As an advantage, the system can be developed to store these data useful for refractory life analysis and preventive maintenance planning.

It should be noted that it is extremely important that the estimate is representative, since the postponement of the refractory change can lead to a perforation in the vessel, causing process stops, production losses and possible accidents. On the other hand, if the replacement is done in advance, the user will not have the total service life of the refractory materials recommended by the supplier. Therefore, it is important to increase the generalizability of the model by covering new refractory wear scenarios.

Acknowledgements. The development of this work was supported by the Postgraduate Program in Control and Automation Engineering (ProPECAut) of the Institute Federal of Espírito Santo (Ifes - Campus Serra). Thanks to the steel company for providing the material used in this work.

Authorship statement. The authors hereby confirm that they are the sole liable persons responsible for the authorship of this work, and that all material that has been herein included as part of the present paper is either the property (and authorship) of the authors, or has the permission of the owners to be included here.

References

[1] F. de M. Torres, "Modelamento físico e matemático dos efeitos da injeção auxiliar de gás em um reator Kanbara," Mestrado, Universidade Federal de Ouro Preto, Ouro Preto, 2017. Accessed: Jun. 13, 2022. [Online]. Available: https://www.repositorio.ufop.br/handle/123456789/7568

[2] W. J. Silveira, "Modelamento matemático do escoamento de fluidos no processo RH para previsão da taxa de circulação do aço," Universidade Federal de Minas Gerais, Belo Horizonte, 2011. Accessed: Jun. 13, 2022. [Online]. Available: http://bdtd.ibict.br/vufind/Record/UFMG_706b99fc7b290996b9cea5582dba0879

[3] A. M. B. Silva, J. J. M. Peixoto, C. A. da Silva, and I. A. Silva, "Steel desulfurization on RH degasser: physical and mathematical modeling," *REM - International Engineering Journal*, vol. 75, no. 1, pp. 27–35, Mar. 2022, doi: 10.1590/0370-44672021750058.

[4] P. H. R. V. de Melo *et al.*, "The influence of flow asymmetry on refractory erosion in the vacuum chamber of a RH degasser," *Journal of Materials Research and Technology*, vol. 8, no. 5, pp. 3764–3771, Sep. 2019, doi: 10.1016/j.jmrt.2019.06.036.

[5] U. A. Vieira, "Modelamento matemático da descarburação do aço líquido em reatores à vácuo RH utilizando o método numérico volumes finitos e o modelo de tanques em série," Doutorado, Universidade Federal do Rio de Janeiro, Rio de Janeiro, 2001.

[6] C. F. de S. Morais, R. da S. Magalhães, A. A. Martins, M. S. A. Pereira, T. A. da Silva, and J. L. Klug, "Implantação da ferramenta 'disponibilidade' no desgaseificador à vácuo da CSN," in *Anais do Seminário de Aciaria, Fundição e Metalurgia de Não-Ferrosos*, Sep. 2017, pp. 272–280. doi: 10.5151/1982-9345-26446.

[7] E. A. Maranhão, "Gerenciamento de riscos e segurança no projeto de um desgaseificador à vácuo RH (Ruhrstahl-Heraeus)," Pós graduação latu senso, Universidade Paulista – UNIP, Santos, 2017. Accessed: Jun. 15, 2022. [Online]. Available: https://89127120-002a-4a5c-ae6f-f89d4bf7270f.filesusr.com/ugd/f72ab0_e82c27d10a5c476d98fae57ee160f449.pdf

[8] A. O. Marchesi, "Análises de falhas em lanças de oxigênio de um desgaseificador a vácuo," Universidade Tecnológica Federal do Paraná, Curitiba, 2019. Accessed: Jun. 15, 2022. [Online]. Available: http://repositorio.roca.utfpr.edu.br/jspui/bitstream/1/18737/1/CT_CEECVIT_II_2019_02.pdf

[9] L. A. S. González, "Towards VisualInertial SLAM for Dynamic Environments Using Instance Segmentation and Dense Optical Flow," Master in Systems, KTH Royal Institute of Technology, Stockholm, 2021.

[10] K. Kutvonen, "Multi-task learning in Computer Vision," Master's Programme in Computer Science, University of Helsinki, Helsinki, 2020. Accessed: Jun. 15, 2022. [Online]. Available: http://www.cs.helsinki.fi/

[11] G. F. E. Tabares, "Machine Learning Image Segmentation to Improve Object Recognition in Mixed Reality," Master of Science, Technical University of Munich, Munich, 2020.

[12] L. Liu *et al.*, "Deep Learning for Generic Object Detection: A Survey," *International Journal of Computer Vision*, vol. 128, no. 2, pp. 261–318, Feb. 2020, doi: 10.1007/s11263-019-01247-4.

[13] K. He, G. Gkioxari, P. Dollar, and R. Girshick, "Mask R-CNN," in *2017 IEEE International Conference on Computer Vision (ICCV)*, Oct. 2017, pp. 2980–2988. doi: 10.1109/ICCV.2017.322.

[14] Y. Li, H. Qi, J. Dai, X. Ji, and Y. Wei, "Fully Convolutional Instance-Aware Semantic Segmentation," in *2017 IEEE Conference on Computer Vision and Pattern Recognition (CVPR)*, Jul. 2017, pp. 4438–4446. doi: 10.1109/CVPR.2017.472.

[15] C.-Y. Fu, M. Shvets, and A. C. Berg, "RetinaMask: Learning to predict masks improves state-of-the-art single-shot detection for free," Jan. 2019, doi: 10.48550/arxiv.1901.03353.

[16] S. Liu, L. Qi, H. Qin, J. Shi, and J. Jia, "Path Aggregation Network for Instance Segmentation," in *2018 IEEE/CVF Conference on Computer Vision and Pattern Recognition*, Jun. 2018, pp. 8759–8768. doi: 10.1109/CVPR.2018.00913.

[17] R. Kanjee, "YOLACT — Real-Time Instance Segmentation," *Medium DataDrivenInvestor*, 19AD. https://medium.datadriveninvestor.com/yolact-real-time-instance-segmentation-5cbe6fc2ba36 (accessed Jun. 15, 2022).

[18] D. Bolya, C. Zhou, F. Xiao, and Y. J. Lee, "YOLACT: Real-Time Instance Segmentation," in *2019 IEEE/CVF International Conference on Computer Vision (ICCV)*, Oct. 2019, pp. 9156–9165. doi: 10.1109/ICCV.2019.00925.

[19] M. D. Bloice, "Augmentor," 2016. https://github.com/mdbloice/Augmentor (accessed Jun. 16, 2022).

[20] L. Mantuan, "Augmentor2RH_Throats," 2022. https://github.com/Lucas-Mantuan/Augmentor2RH_Throats (accessed Jun. 16, 2022).